nature communications

Article

https://doi.org/10.1038/s41467-024-53866-2

Hippocampal contextualization of social rewards in mice

Received: 8 May 2023

Accepted: 22 October 2024

Published online: 03 November 2024

Check for updates

Joana Mendes Duarte[1,2,4], Robin Nguyen[1,3,4], Marios Kyprou[1], Kaizhen Li[1], Anastasija Milentijevic[1], Carlo Cerquetella[1], Thomas Forro[1] & Stéphane Ciocchi[1]

Acquiring and exploiting memories of rewarding experiences is critical for survival. The spatial environment in which a rewarding stimulus is encountered regulates memory retrieval. The ventral hippocampus (vH) has been implicated in contextual memories involving rewarding stimuli such as food, social cues or drugs. Yet, the neuronal representations and circuits underlying contextual memories of socially rewarding stimuli are poorly understood. Here, using in vivo electrophysiological recordings, in vivo one-photon calcium imaging, and optogenetics during a social reward contextual conditioning paradigm in male mice, we show that vH neurons discriminate between contexts with neutral or acquired social reward value. The formation of context-discriminating vH neurons following learning was contingent upon the presence of unconditioned stimuli. Moreover, vH neurons showed distinct contextual representations during the retrieval of social reward compared to fear contextual memories. Finally, optogenetic inhibition of locus coeruleus (LC) projections in the vH selectively disrupted social reward contextual memory by impairing vH contextual representations. Collectively, our findings reveal that the vH integrates contextual and social reward information, with memory encoding of these representations supported by input from the LC.

The survival of animals depends on their ability to access and use memories of rewarding and aversive experiences[1]. Memory-guided behaviour depends on the brain's capacity to simultaneously construct internal representations of salient emotional experiences and spatial environments in which these experiences occur. In particular, learning about social cues is adaptive as it enables individuals to locate predators, resource competitors, and reproductive mates[2]. Certain social cues can act as unconditioned stimuli that motivate and reinforce behaviour. For instance, male and female rodents learn to approach and preferentially occupy environments (i.e., contexts) that had previously contained cues of the opposite sex[2–4]. While the neuronal mechanisms involved in the processing of social cues have been largely investigated[5–7], the neuronal circuits and representations underlying contextual memories related to social cues remain poorly understood.

The vH is a brain region involved in encoding and retrieving affective memories[8], and mediates behavioural responses associated with positive and negative states[9–15]. Specifically, vH neurons respond to affective zones within a behavioural arena and exhibit large place fields that map onto contexts[16–19]. Furthermore, disrupting vH activity in learning tasks with positive and negative unconditioned stimuli impairs memory, such as during contextual reward conditioning[12,15], social recognition[13,20,21], and context-dependent fear conditioning[14,22,23]. Moreover, neuronal populations within the vH are known to send

[1]Laboratory of Systems Neuroscience, Department of Physiology, University of Bern, Bern, Switzerland. [2]Present address: Roche Pharma Research and Early Development, Roche Innovation Center Basel, F. Hoffmann-La Roche AG, Basel, Switzerland. [3]Present address: Department of Neuroscience, The Kavli Institute for Brain Science, Mortimer B. Zuckerman Mind Brain Behavior Institute, Jerome L. Greene Science Center, Columbia University, New York, NY, USA. [4]These authors contributed equally: Joana Mendes Duarte, Robin Nguyen. e-mail: stephane.ciocchi@unibe.ch

afferents to and receive afferents from a variety of brain regions involved in innate and conditioned behaviours[24,25]. Together, these findings implicate the vH as a core structure mediating context-dependent emotional behaviours receiving convergent spatial and salience information.

The vH receives neuromodulatory inputs from several brain regions that may be involved in regulating synaptic plasticity mechanisms underlying learning[26]. Of note, the locus coeruleus (LC) is recruited by salience or novelty[27,28], and is a major source of both noradrenaline and dopamine in the hippocampus[28–31]. Noradrenergic signalling enhances CA1 long-term potentiation[32–36], and LC inputs to the dorsal hippocampus facilitate spatial and contextual learning[28,29], support the enrichment of place cells near reward zones[37], and the linking of temporally distinct contextual memories[38], including place-reward learning[39]. The function of LC projections to the vH, on the other hand, has not yet been explored.

In the present study, we examined the activity of vH neurons using in vivo single-unit electrophysiological recordings and calcium imaging combined with optogenetic manipulations of the LC in mice during a social reward contextual memory paradigm. Our findings indicate that the vH is critical for associating contexts with social rewards via a process dependent on LC activity.

Results

The vH discriminates contexts following social reward contextual conditioning

The vH has been shown to encode contexts associated with natural rewards[40–42], including social rewards[12]. To identify the neuronal correlates of contextual memory for social reward in the vH, we subjected male mice (3–5 months old, $n = 23$, C57BL6/J) to a conditioned place preference task (CPP) using social-odour reward, while performing chronic single-unit electrophysiological recordings (Fig. 1a, b and Supplementary Fig. 1). Mice were first habituated (Pre-Train Test) to a maze with two chambers with different features (i.e., contexts A and B) connected by a central alley. Then, throughout three consecutive training sessions separated by 1 h, mice were placed into the maze with context B containing a neutral odour (clean rodent bedding mixed with 1% cinnamon) and context A containing female odour (i.e., home-cage bedding of adult females containing female odours and pheromones) which acted as a conditioned reinforcer. We previously tested that the clean bedding mixed with 1% of cinnamon did not induce a preference or an aversion in a place preference task (Supplementary Fig. 2C). Fourteen hours following training, mice were re-exposed to the maze – in the absence of added odours – to test social reward CPP memory (Post-Train Test). Memory strength was measured by the

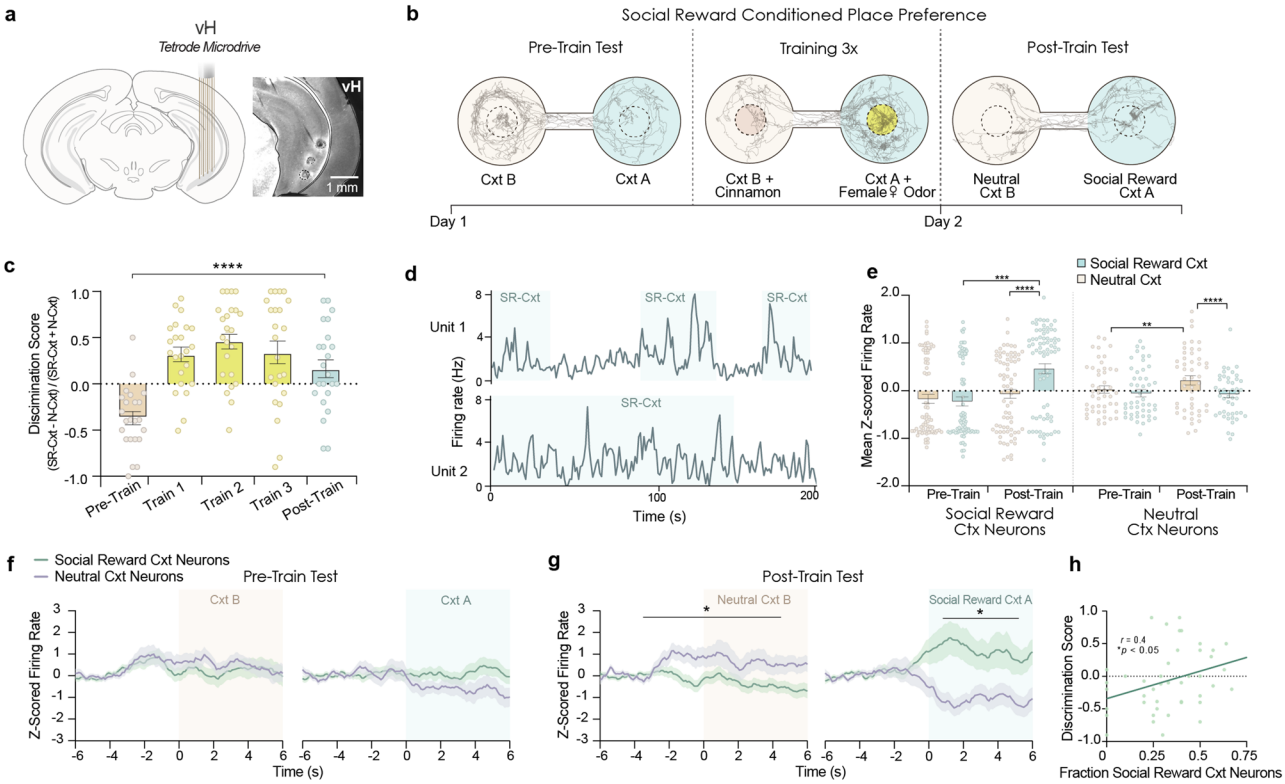

Fig. 1 | The vH discriminates contexts following social reward contextual conditioning. a Schematic and image of vH tetrode microdrives. **b** Experimental design of social reward (SR) CPP task with representative trajectories. **c** Context discrimination score per session. Repeated measures (RM) one-way ANOVA $F_{(2.8,61.8)} = 18.55$, $P = 2.1 \times 10^{-8}$. Pre-Train vs. Train-1 $P = 7.9 \times 10^{-7}$, Train-2 $P = 2.9 \times 10^{-7}$, Train-3 $P = 1.9 \times 10^{-6}$, Pre- vs. Post-Train $P = 5.3 \times 10^{-6}$. One-sample t-test vs. zero, Pre-Train $t_{(22)} = 5.19$ $P = 1.7 \times 10^{-5}$, Train-1 $t_{(22)} = 4.1$ $P = 0.0006$, Train-2 $t_{(22)} = 5.22$ $P = 1.5 \times 10^{-5}$, Train-3 $t_{(22)} = 2.8$ $P = 0.0104$, Post-Train $t_{(22)} = 1.7$ $P = 0.103$. **d** Firing rate of two SR-context neurons at Post-Train. **e** Normalized firing rate of context neurons at Pre- and Post-Train. Two-way RM-ANOVA, SR-context neurons: session × context, $F_{(1,73)} = 22.52$, $P = 0.00001$; SR-context Pre- vs. Post-Train $P = 1.64 \times 10^{-11}$; Post-Train SR- vs. neutral-context $P = 4.07 \times 10^{-8}$, $n = 74$ neurons. One-sample t-test, Pre-Train SR-context $t_{(73)} = 2.34$ $P = 0.022$; Post-train SR-context $t_{(73)} = 4.45$ $P = 0.00003$. Two-way RM-ANOVA, neutral-context neurons: context, $F_{(1,46)} = 19.78$ $P = 0.000055$; Post-Train SR- vs. neutral-context $P = 5.11 \times 10^{-6}$; neutral-context Pre- vs. Post-Train $P = 0.0072$, $n = 47$ neurons. **f** Normalized firing rate of SR- and neutral-context neurons upon entry into context-B or -A at Pre-Train: context-B, −2 to −1s, neutral-context neurons, $t_{(45)} = 2.11$ $P = 0.041$; SR-context neurons, $t_{(67)} = 2.46$ $P = 0.017$, and during (**g**) Post-Train: three-way Mixed-ANOVA, pre-entry group × context × time, $F_{(3.7,\ 448.5)} = 3.94$ $P = 0.005$; post-entry group x context: $F_{(1,120)} = 12.65$ $P = 0.0005$. One-sample *t*-test, pre-entry into neutral-context, neutral-context neurons: −2 to −1 s, $t_{(47)} = 3.01$ $P = 0.004$; −1 to 0 s, $t_{(47)} = 2.19$ $P = 0.034$; pre-entry into SR-context, SR-context neurons: −2 to −1 s, $t_{(73)} = 0.89$ $P = 0.38$; −1 to 0 s, $t_{(73)} = 2.39$ $P = 0.02$. **h** Correlation between context discrimination and proportion of SR-context neurons during Post-Train. Pearson's *r* (2-tailed), $r = 0.4$ $P = 0.0141$. All multiple-comparisons were Bonferroni-corrected 2-tailed *t*-tests. Data are from $n = 23$ mice. Bar charts are presented as mean ± SEM.

https://doi.org/10.1038/s41467-024-53866-2

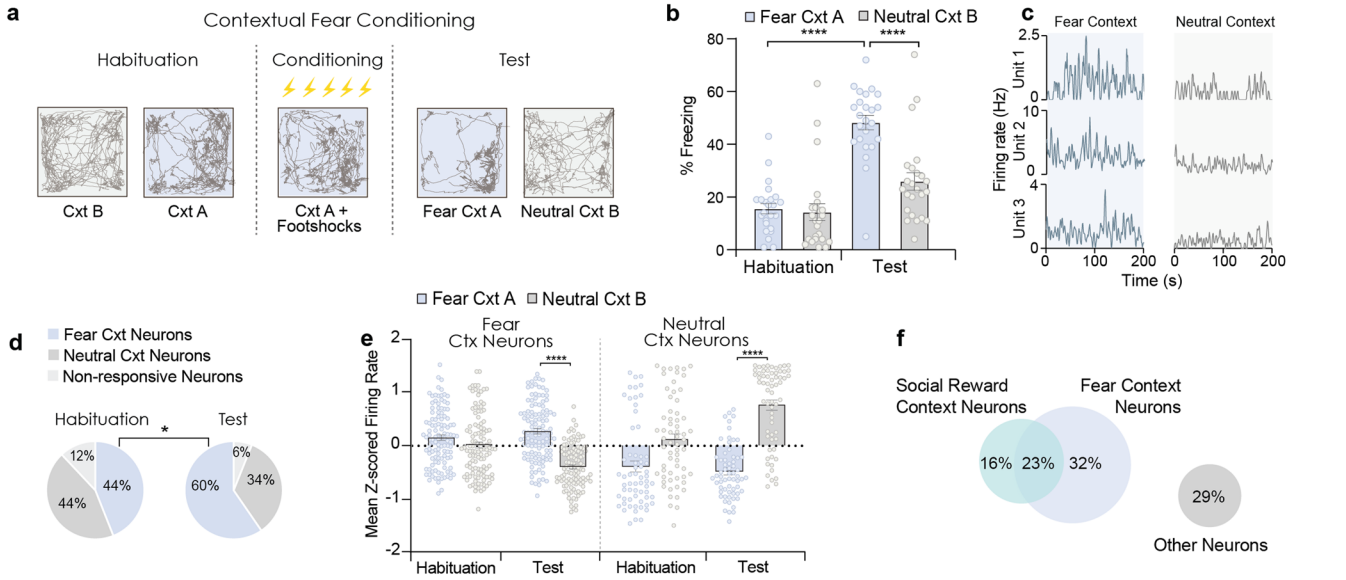

Fig. 2 | The vH represents emotional contexts in a valence-specific manner. **a** Behavioural protocol and representative mouse trajectories during the habituation, fear conditioning and test sessions for the contextual fear memory task. **b** Freezing levels during habituation and test sessions. Two-way RM ANOVA between groups, context × session $F_{(1,23)} = 20.20$, $P = 0.0002$. Context-A vs. context-B during test $P = 4.2 \times 10^{-6}$, and habituation vs. test at context-A $P = 5.7 \times 10^{-9}$, $n = 24$ mice. **c** Example firing rate traces of fear context neurons at the habituation and test sessions in context-A and -B. **d** Comparison of neuron proportions at habituation and test sessions. Chi-squared test between sessions, $P = 0.0235$, $n = 24$ mice. **e** Averaged normalized firing rates during habituation and test sessions in context-A and -B for fear (left) and neutral context neurons (right). Two-way RM ANOVA, fear context neurons: session × context $F_{(1,113)} = 53$, $P = 1 \times 10^{-11}$. Context-A vs. Context-B at the Test session $P = 1 \times 10^{-16}$, $n = 114$ neurons, $n = 24$ mice. Neutral context neurons: session × context $F_{(1,62)} = 15.41$, $P = 0.00022$. Context-A vs. Context-B at the Test session, $P = 4.8 \times 10^{-13}$ $n = 64$ neurons, $n = 24$ mice. **f** Overlap of neurons with preferential activity in the social reward context and fear context. Hypergeometric test 2-sided, $OR = 1.1$, $P = 0.273$; Fisher exact test 2-sided $P = 0.509$; $n = 154$ neurons in total, $n = 23$ mice. All multiple-comparisons were Bonferroni-corrected 2-tailed t-tests. Data are presented as the mean ± SEM.

degree of preference for the context previously paired with female odour (social reward context) over the context previously paired with neutral odour which was calculated as a discrimination score using the time spent in each context of the maze (Fig. 1c). During training, mice exhibited a strong preference for the context and zone paired with social reward (Fig. 1c and Supplementary Fig. 2A, B). This preference was maintained during the Post-Train Test session and was elevated compared to the Pre-Train Test session, indicating that mice formed a place preference memory. Next, we determined whether individual vH neurons display differential firing rates when mice occupied the neutral versus social reward context at the Post-Train Test session. Neurons were categorized based on their context preference – social reward, neutral, or non-preferring—using permutation testing with bootstrapping. Firing rates across time within each context were initially extracted and the mean differences computed. Time bins were subsequently shuffled, resampled with replacement, and mean differences computed with the process repeated across 1000 iterations to establish a null distribution. Statistical significance was assessed by comparing the actual mean differences against this null distribution. All well-isolated units were included in the analysis. We found that during the Post-Train Test session, 40% of vH neurons exhibited higher overall activity in the social reward context than in the neutral context (Fig. 1d, e), while 26% were preferentially active in the neutral context. This preferential activity was seen in their mean firing rate in the preferred context at the Post-Train but not at the Pre-Train Test session (Fig. 1e). Context neurons also exhibited increased activity upon entering their preferred context at the Post-Train Test session (Fig. 1g, Supplementary Fig. 2D), but only after training (Fig. 1f, g). Furthermore, context neurons displayed anticipatory activity, firing 1–2 s prior to context entry (Fig. 1f, g). These firing rate patterns are unlikely to relate to movement since the activity of context neurons was not correlated with locomotor speed (Supplementary Fig. 2F). Moreover, we found that preference for the social reward context at the behavioural level was correlated with the proportion of social reward context neurons (Fig. 1h), suggesting that vH neuronal activity representing the social reward context supports memory retrieval. This correlation was absent for vH neurons that were preferentially active in the neutral context (Supplementary Fig. 2G). To further confirm that the activity of social reward context neurons carried selective information about the context, we decoded the context identity from the firing rates of individual mice using a linear support vector machine (SVM) classifier. We found that the classification accuracy was higher with a model trained on correct compared to randomized labels (Supplementary Fig. 2E). Additionally, as a consequence of learning, we observed that a subset of social reward context neurons enhanced their firing when mice entered into the social reward zone during the Post-Train Test session (Supplementary Fig. 2H) in parallel with an increase in their proportion (Supplementary Fig. 2I). Together, these findings indicate that the vH discriminates contexts following social reward contextual conditioning.

The vH represents emotional contexts in a valence-specific manner

Next, we asked whether vH contextual representations may differ according to valence. To address this question, we subjected mice to a discriminative contextual fear conditioning procedure involving two contexts: context A in which mice received electrical foot shocks and context B where no foot shocks were delivered ($n = 24$ mice, Fig. 2a). Following contextual fear conditioning, mice exhibited high freezing levels in context A at the memory test session whereas freezing levels in context B remained low, indicating that mice formed a selective contextual fear memory (Fig. 2b).

An examination of the contextual representations at the memory test session revealed that the majority of vH neurons were selectively active in context A (corresponding to fear context neurons) concomitant with an increase in the fraction of vH neurons representing

context A compared to the habituation session (Fig. 2c, d). During the memory test session, fear context neurons showed increased firing selectively in context A compared with context B, which was not observed during habituation (Fig. 2e). Additionally, 24% of these neurons are activated by the shock during the training session (Supplementary Fig. 3C). This finding suggests that, similar to our findings with social reward contextual conditioning, the vH preferentially represents the emotional context after learning. Of note, the activity of vH neurons was not correlated with the speed of movement during contextual fear conditioning (Supplementary Fig. 3A). Moreover, using a SVM to decode context identity in individual mice, we found that the classification accuracy was higher for the model trained on correct compared to randomized labels suggesting context was also represented at the population level (Supplementary Fig. 3B). To determine if the presence of an aversive stimulus was necessary for the formation of context-discriminating activity and memory in the vH, a control paradigm using a neutral stimulus (i.e., two foot shocks of 0.06 mA) was conducted in a separate cohort of mice ($n = 6$ mice, Supplementary Fig. 3D). Mice did not exhibit a contextual fear memory during this mock conditioning (Supplementary Fig. 3E), but when subjected to the classical contextual fear conditioning, they expressed contextual fear memory associated with the formation of fear context neurons (Supplementary Fig. 3F, G). This indicates that selective contextual representations are formed in the vH following contextual fear conditioning.

Finally, we examined the extent to which context-discriminating vH neurons overlapped in the social reward and fear paradigms. We found that a relatively small proportion of vH neurons (23%) exhibited social reward and fear context activity in both paradigms, which did not significantly differ from chance-level, while a larger proportion of neurons were selectively active in the social reward or fear contexts (48%). This suggests that the vH can discriminate contexts associated with social reward and fear by two independent neuronal mechanisms (Fig. 2f).

Activity of social reward context neurons is contingent on social reward association

The selective contextual activity observed in the vH may result from an associative emotional experience or reflect a non-associative process such as contextual sensitization or the mere passage of time. To evaluate if the presence of the unconditioned social reward was essential for the development of context-discriminating activity, a Mock CPP paradigm involving only neutral odours was conducted in a separate cohort of mice ($n = 9$ mice) followed by the classical social reward CPP (Fig. 3a). In the Mock CPP paradigm, mice showed higher variability in time spent in the two contexts during training, and no change in context preference between the Pre- and Post-Train Tests (Fig. 3b, d). This contrasts with behaviour in the social reward CPP paradigm, in which mice increased their preference for the social reward context between the Pre- and Post-Train Tests (Fig. 3b, d). Then, we classified neurons as social reward and neutral context neurons according to their context selectivity at the social reward CPP Post-Train Test and examined their activity at the Mock CPP Post-Train Test. We found that context neurons exhibited increased activity in their selective context in the social reward CPP paradigm but showed no context discrimination as a population in the Mock CPP paradigm (Fig. 3c, e, f). These findings were not explained by behavioural preference for the social reward context in the social reward CPP paradigm (Supplementary Fig. 4B). Thus, both social reward contextual memory and the accompanying vH contextual representations rely on salient reinforcers during associative learning.

Learning enhances representation of the social reward context

Next, we investigated whether the encoding of context-social reward associations involves changes in vH contextual activity across learning. Comparing the context-specific activity of vH neurons between the Pre- and Post-train tests in the social reward CPP task, we found a significant increase in the percentage of social reward context-responsive neurons at post-training (Fig. 4a). To understand the underlying neuronal dynamics, we analysed shifts in neuronal responses from pre- to post-training. We observed that a large percentage of neurons that had preferred the social reward context at pre-training maintained their preference at post-training, indicating the maintenance of existing representations of the social reward context (Fig. 4b). Additionally, a substantial proportion of neurons that initially showed no context preference went on to prefer the social reward context, while many neurons that had preferred the neutral context became non-discriminating, highlighting a reorganization of neuronal activity towards the social reward context and away from the neutral context (Fig. 4b). Spatial firing patterns further supported these observations. At post-training, social reward context neurons displayed place fields that broadly encompassed the social reward context (Supplementary Fig. 4A, C), consistent with previous reports of context-related spatial activity in the vH[18,19,43]. Neurons that preferred the social reward context at both pre- and post-training showed positively correlated spatial firing rate maps while neurons that were non-discriminating or that preferred the neutral context at pre-training exhibited no or negative correlations, respectively (Supplementary Fig. 4C, D). We observed the same trends for neutral context neurons (Supplementary Fig. 4E, F). These results indicate that vH neurons form a biased representation of the social reward context following learning, through a coordinated response involving both the maintenance and reorganization of neuronal activity.

While social reward context representations in the vH were found to emerge after learning, it is unclear if vH activity during learning is causally related to these representations and to contextual memory. We addressed this question by first evaluating the requirement of vH activity for the encoding of social reward contextual memory. We used optogenetics to inhibit vH pyramidal neurons during the training phase of the social reward CPP task. Mice were infused with adeno-associated virus (AAV) containing the inhibitory opsin archaerhodopsin (eArch3.0) under the control of the CaMKIIα promoter and implanted with optic fibres in the vCA1 (Fig. 4c). Laser light was delivered whenever mice occupied the social reward context during the training sessions (Fig. 4d). There was no immediate effect of light inhibition on context preference, indicating that vH inhibition did not alter social reward seeking behaviour (Fig. 4e). However, during the Post-train test, vH-eArch3.0 mice exhibited less preference for the social reward context compared to vH-EYFP control mice and did not significantly change their preference relative to the Pre-train test (Fig. 4f). These findings suggest that the inhibition of vH pyramidal neurons during training prevented the formation of social reward contextual memory.

Next, we sought to determine if vCA1 activity during learning is required for the emergence of social reward contextual representations. We therefore silenced vH pyramidal neurons during learning and assessed the impact on social reward context activity during the memory test. This was achieved using dual-colour head-mounted miniature microscopes to perform one-photon calcium imaging from vCA1 pyramidal neurons. AAV vectors containing GCaMP6f or the inhibitory opsin halorhodopsin (eNpHR3.0) both driven by the CaMKIIα promoter were unilaterally infused into the vH and a gradient refractive index (GRIN) lens was implanted above the injection site in the vCA1 pyramidal layer (Fig. 4g). Calcium imaging was performed during Pre- and Post-train test sessions while optogenetic inhibition occurred during training sessions when mice occupied the social reward context (Fig. 4d)[44,45]. Similar to the findings we obtained with electrophysiological recordings, our calcium imaging recordings revealed context-selective neurons in the vH of both control vH-GCaMP6f-tdTomato and vH-GCaMP6f-eNpHR3.0 mice (Fig. 4h).

https://doi.org/10.1038/s41467-024-53866-2

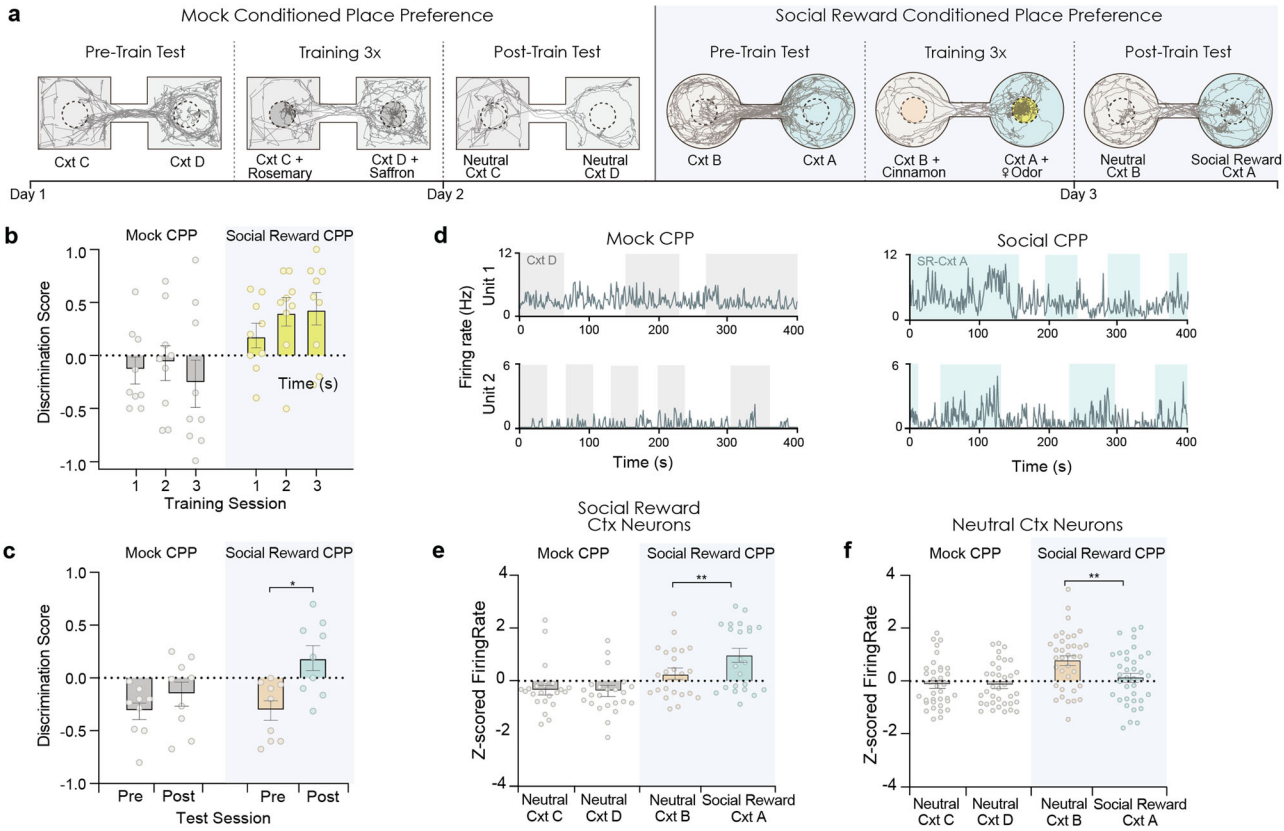

Fig. 3 | Emergence of social reward context neurons is contingent on associative learning. a Experimental design of Mock and Social Reward CPP with representative mouse trajectories. **b** Discrimination scores during training. Two-way RM-ANOVA, task effect $F_{(1,8)} = 4.9$, $P = 0.0577$. One-sample t-test 2-tailed, SR-CPP Train-2 $t_{(8)} = 3.07$ $P = 0.0153$; Train-3 $t_{(8)} = 2.86$ $P = 0.0212$; all other comparisons non-significant, $n = 9$ mice. **c** Discrimination scores during Pre- and Post-Train Tests in the context that was non-preferred at Pre-train for Mock- and SR-CPP. Two-way RM-ANOVA, task effect $F_{(1,8)} = 7.23$ $P = 0.0275$, session × task $F_{(1,8)} = 9.07$ $P = 0.0168$. SR-CPP Pre- vs. Post-Train $P = 0.007$. One-sample t-test 2-tailed, Mock-CPP Pre $t_{(8)} = 3.78$ $P = 0.0054$; Post $t_{(8)} = 1.31$, $P = 0.228$; SR-CPP Pre $t_{(8)} = 3.28$, $P = 0.0112$; Post $t_{(8)} = 1.54$ $P = 0.16$, $n = 9$ mice. **d** Representative firing rate traces of two SR-context neurons. **e** Normalized firing rate of social reward context neurons during the Post-train Test. Two-way RM-ANOVA, context $F_{(1,22)} = 8.351$ $P = 0.0085$; task $F_{(1,22)} = 10.08$ $P = 0.0044$. SR-CPP comparison of SR vs. neutral context $P = 0.0055$. One-sample t-test 2-tailed, neutral-context-C $t_{(22)} = 1.6$ $P = 0.12$, neutral-context-D $t_{(22)} = 2.89$ $P = 0.0085$; neutral-context-B $t_{(22)} = 1.5$, $P = 0.16$; SR-context-A $t_{(22)} =$ $P = 0.0013$; $n = 23$ neurons, 9 mice. **f** Normalized firing rate of neutral context neurons during Post-train. Two-way RM-ANOVA, context $F_{(1,35)} = 6.62$ $P = 0.0145$; task $F_{(1,35)} = 7.4$ $P = 0.0101$; context vs. task $F_{(1,35)} = 7.13$ $P = 0.0114$. SR CPP SR vs. neutral context, $P = 0.0049$. One-sample t-test 2-tailed, neutral-context-C $t_{(35)} = 0.92$ $P = 0.364$; neutral-context-D $t_{(35)} = 1.15$ $P = 0.257$; neutral-context-B $t_{(35)} = 4.27$ $P = 0.0001$; SR-CtxA $t_{(35)} = 0.79$ $P = 0.437$; $n = 36$ neurons, 9 mice. All multiple-comparisons were Bonferroni-corrected 2-tailed *t*-tests. Data are presented as the mean ± SEM.

Furthermore, vH-GCaMP6f-tdTomato mice exhibited an increased percentage of social reward context neurons post-training compared to pre-training (Fig. 4i), as described earlier (Fig. 4a). Notably, vH-GCaMP6f-eNpHR3.0 mice showed no change in proportions of context-selective neurons across learning and fewer social reward context neurons at the Post-train test compared to vH-GCaMP6f-tdTomato mice. We then tracked the changes in context selectivity of individual neurons between the Pre- and Post-train tests. We found that among the neurons with no context preference pre-training, fewer went on to prefer the social reward context post-training in vH-GCaMP6f-eNpHR3.0 mice compared to vH-GCaMP6f-tdTomato mice (Fig. 4j). This finding suggests that vH inhibition during associative learning disrupted the shift in contextual activity towards the social reward context. Moreover, when we examined the activity of context-selective neurons upon entry into their preferred contexts, we noticed that both social reward and neutral context neurons in eNpHR3.0 mice displayed a dramatically reduced magnitude of activation following context entry (Fig. 4k–l). Taken together, these results indicate that social reward contextual memory depends on vH activity during the encoding of context-social reward associations, achieved through the active enhancement of social reward context representations.

vH neurons represent social reward

We observed that the vH reorganizes its contextual activity following exposure to female odour. We next asked whether vH neurons respond to female odour itself and if this activity is a response to the rewarding or social nature of the stimulus. To address this, we performed calcium imaging from the vH as mice explored two-chamber mazes containing a neutral stimulus in one context and an unconditioned stimulus in the other context, specifically food reward (sucrose pellets), female odour, or a female conspecific (Fig. 5a). We identified vH neurons that were activated by each unconditioned stimulus relative to the neutral stimulus (Fig. 5b), with 31% activated by female odour, 27% by sucrose, and 36% by female conspecific. Compared to non-activated neurons, sucrose-activated and female conspecific-activated neurons showed a higher likelihood of being activated by female odour (Fig. 5c), and responses to both stimuli were positively correlated with responses to female odour (Fig. 5g). In contrast, activation by female conspecific was as expected by chance among sucrose-activated neurons (Fig. 5d), and responses to these two stimuli were not significantly correlated. These findings indicate that food reward and female conspecific are independently represented in the vH, while female odour representations overlap with both reward and social representations. We also assessed whether female odour activity

https://doi.org/10.1038/s41467-024-53866-2

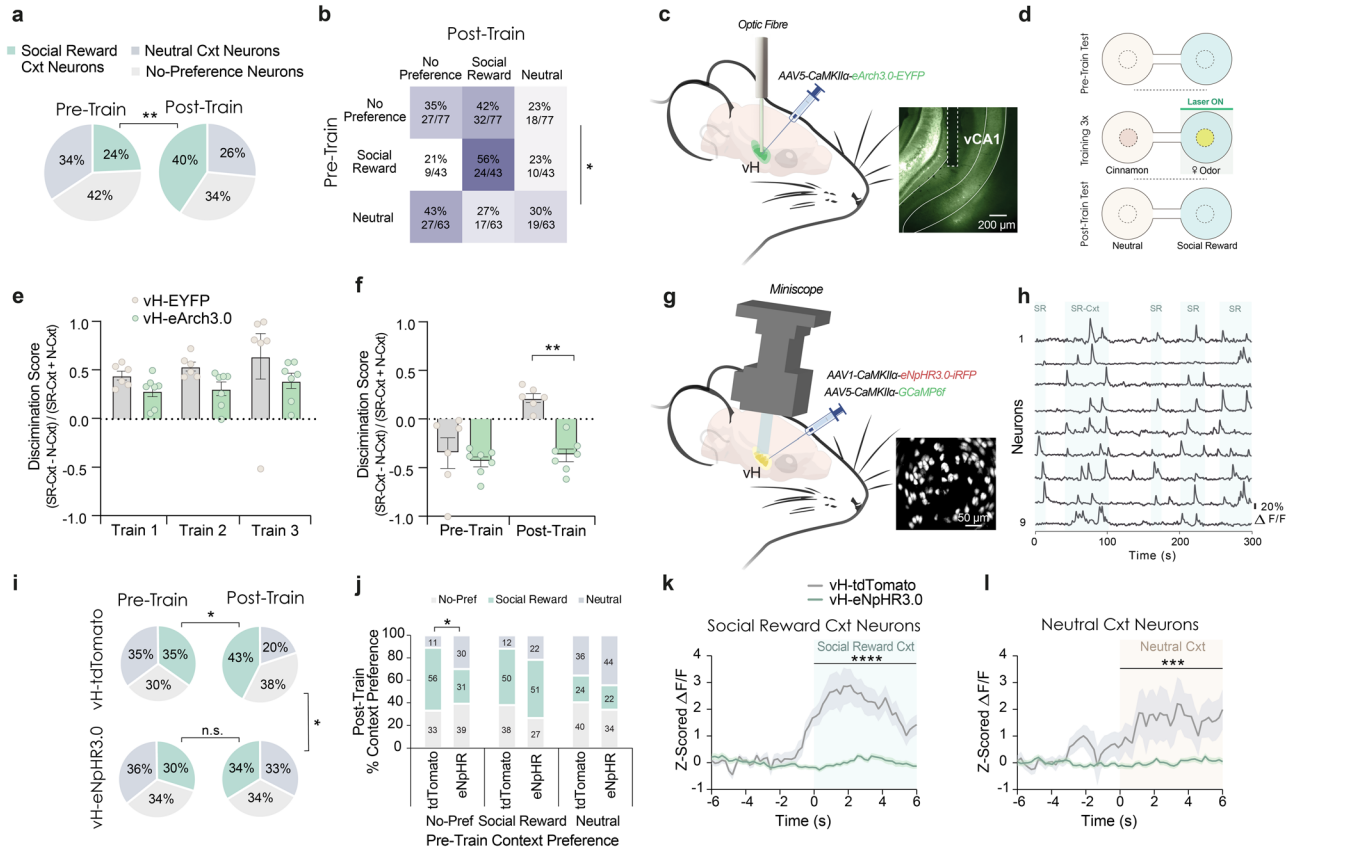

Fig. 4 | Ventral hippocampal neurons reorganize their context activity upon social reward contextual learning. a Percentages of context neurons at Pre- and Post-Train. Chi-squared test, $\chi^2_{(2)} = 11.26$ $P = 0.0036$, $n = 23$ mice. **b** Contingency matrix of neuron percentages and counts per context category at Pre- and Post-Train. $\chi^2_{(4)} = 9.75$, $P = 0.0448$, $n = 23$ mice. **c** Schematic and example image of optogenetic strategy. **d** Schematic of SR-CPP task with laser illumination in SR-context during training. (C-F) $n = 6$ EYFP, $n = 7$ eArch3.0. **e** Behavioural discrimination score during training. Two-way Mixed-ANOVA, group effect $F_{(1,6)} = 7.617$ $P = 0.0329$; **f** Discrimination score during Pre- and Post-Train. Two-way Mixed-ANOVA, group × session $F_{(1,4)} = 40.98$, $P = 0.0031$. Bonferroni-corrected comparisons, Post-Train EYFP vs. eArch3.0, $P = 0.0048$. **g** Schematic of calcium imaging strategy. Inset, processed 1-photon Ca^{2+} signals in vH pyramidal neurons. (G-N) tdTomato: $n = 120$ neurons, 2 mice; eNpHR3.0: $n = 273$ neurons, 3 mice. **h** Representative Ca^{2+} traces of SR-context neurons during SR-CPP at Post-Train. **i** Percentages of context neurons during Pre- and Post-train. tdTomato: $\chi^2_{(2)} = 6.78$ $P = 0.0337$; eNpHR3.0: $\chi^2_{(2)} = 0.94$ $P = 0.625$. **j** Contingency table of neurons in each context category at Pre-Train and percentage at Post-Train. Numbers indicate percentages of neurons. Non-preferring at Pre-train: $\chi^2_{(2)} = 8.15$ $P = 0.017$; SR-preferring at Pre-train: $\chi^2_{(2)} = 2.67$ $P = 0.263$; neutral-preferring at Pre-train: $\chi^2_{(2)} = 0.92$ $P = 0.631$. **k** Z-scored Ca^{2+} activity of SR-context neurons upon entry into SR-context at Post-Train. Two-way Mixed-ANOVA, pre-entry group × time $F_{(4.6,644.8)} = 8.27$ $P = 3.97 \times 10^{-7}$; post-entry group $F_{(1,141)} = 49.52$ $P = 7.87 \times 10^{-11}$. **l** Z-scored Ca^{2+} activity of neutral-context neurons upon entry into the neutral context at Post-Train. Two-way Mixed-ANOVA, pre-entry group × time: $F_{(3.95,438.7)} = 3.48$ $P = 0.008$; post-entry group: $F_{(1,111)} = 16.19$ $P = 0.00011$. Data are presented as the mean ± SEM.

is distinct from activity in response to aversive stimuli, specifically predator odour and electrical footshocks (Fig. 5a, b). We found that 27% of neurons were activated by fox odour, and 16% by footshock. Compared to non-activated neurons, fox odour-activated neurons were less likely to be activated by female odour (Fig. 5e), and these responses were negatively correlated (Fig. 5g), suggesting these stimuli have opposing effects on a subset of neurons. Lastly, similar to what we observed with contextual activity (Fig. 2f), the proportion of female odour-activated neurons among shock-activated neurons did not differ from chance level, and responses to these stimuli were not significantly correlated. These results demonstrate that vH neurons respond to stimuli with positive and negative valence, as well as social stimuli, with female odour representations possessing both rewarding and social properties.

Social reward contextual memory involves locus coeruleus projections to the vH

Next, we addressed the potential neuromodulatory inputs to the vH that may play a role in regulating the formation of contextual associations. Since the locus coeruleus (LC) has been implicated in facilitating spatial learning[28,29], and supporting the enrichment of place cells near reward zones[39], we investigated whether LC afferents to the vH may be necessary for social reward contextual learning. In tyrosine hydroxylase (TH)-Cre mice, the LC was bilaterally injected with a Cre-dependent AAV carrying eArch3.0, and optic fibres were implanted in the vH to optogenetically silence LC terminals (Fig. 6a, b and Supplementary Figs. 5A, 6C). Mice underwent the social reward CPP task with light delivery during training sessions upon entry and occupation of the social reward context (Fig. 6c). Optogenetic inhibition of LC terminals in the vH did not immediately affect the time spent in the social reward context or the social reward zone during training, as indicated by similar discrimination scores between LC-vH-EYFP and LC-vH-eArch3.0 mice (Fig. 6d and Supplementary Fig. 5B). However, inhibiting LC activity in the vH during training resulted in a significant decrease in the preference for the social reward context at the Post-Train Test session (Fig. 6e and Supplementary Fig. 5B), suggesting impaired social reward contextual memory. These results point to the necessity of LC projections to the vH in associating social reward stimuli with contextual information. To test for a valence-specific effect, we evaluated the impact of optogenetically suppressing LC terminal

https://doi.org/10.1038/s41467-024-53866-2

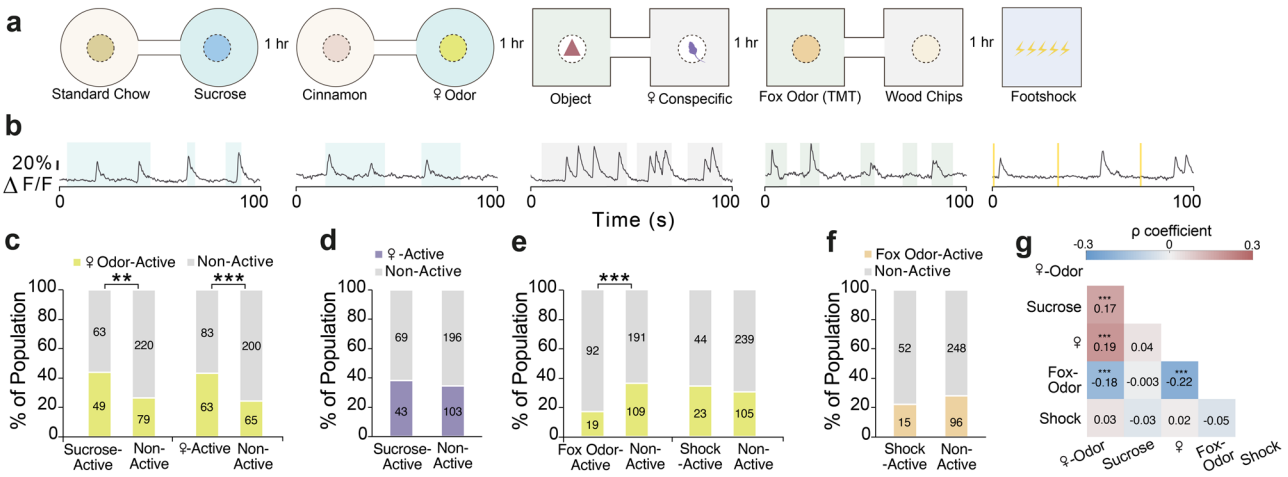

Fig. 5 | Neurons activated by female odour encode food reward and female conspecifics. a Schematic of behavioural paradigm for the presentation of unconditioned stimuli (US). **b** Representative calcium traces of neurons activated by each US in the schematic above. Shaded area indicates periods in stimulus context or foot-shock presentation. **c**–**f** Counts of neurons that were activated and not activated by unconditioned stimuli. Significance was tested by 2-sided Fisher's exact test. **c** Counts of female odor-active, and non-active neurons between sucrose-active and sucrose non-active neurons: $P = 0.0012$, and between female-active and female non-active neurons: $P = 0.0001$. **d** Counts of female conspecific-active, and non-active neurons between sucrose-active and sucrose non-active neurons: $P = 0.488$. **e** Counts of female odor-active, and non-active neurons between fox odor-active and fox odor non-active neurons: $P = 0.0002$, and between shock-active and shock non-active neurons: $P = 0.565$. **f** Counts of fox odor-active, and non-active neurons between shock-active and shock non-active neurons: $P = 0.452$. **g** Matrix of Spearman's rank correlation coefficient ρ (2-tailed) for the response activation to female-odor vs. sucrose: $P = 0.0007$, female-odor vs. female conspecific: $P = 0.0001$, female-odor vs. fox-odor: $P = 0.0002$, female conspecific vs. fox-odor: $P = 0.0001$. $N = 411$ neurons, 5 mice.

activity in the vH during contextual fear conditioning in mice previously tested in the social reward CPP task. However, no significant changes in contextual fear memory were observed (Supplementary Fig. 6A,B).

To evaluate the effect of inhibiting LC afferents on vH neuronal activity, we employed the same optogenetic strategy combined with acute single-unit electrophysiological recordings in the vCA1 of awake head-fixed mice (Fig. 6f). We observed that laser illumination altered vH neuronal activity, increasing both excitatory and inhibitory responses in LC-vH-eArch3.0 mice compared to controls (Fig. 6g–i).

We hypothesized that LC projections to the vH may support the encoding of social reward contextual memory by regulating vH context-selective activity. To test this hypothesis, we performed calcium imaging of vH pyramidal neurons together with optogenetic inhibition of LC terminals in the vH as mice behaved in the social reward CPP task. TH-Cre mice were unilaterally injected with a Cre-dependent AAV carrying eNpHR3.0 into the LC, combined with a second unilateral AAV injection in the vH to express GCaMP6f driven be the CaMKIIα promoter, and a GRIN lens was implanted in the vCA1 (Fig. 6j, k and Supplementary Fig. 5C). LC projections in the vH were inhibited as mice entered and occupied the social reward context during the social reward CPP training sessions. Examining activity at the Post-train test, we observed context-selective neurons in both LC-vH-tdTomato and LC-vH-eNpHR3.0 mice (Fig. 6l–n). However, LC-vH-eNpHR3.0 mice had a significantly smaller percentage of social reward context neurons compared to LC-vH-tdTomato mice (Fig. 6m). Furthermore, the activity of both social reward and neutral context neurons upon entry into their preferred context was lower in LC-vH-eNpHR3.0 mice (Fig. 6n). Collectively, these results suggest that the LC facilitates social reward contextual memory formation by promoting the activity of social reward context neurons in the vH.

Discussion

We found that the vH supports the formation of contextual memory for social rewards by generating context-specific representations. These representations emerged upon learning, depended on the presence of social reward, and involved a preferential reorganization of context-selective activity towards the social reward context. A circuit-based strategy identified LC projections to the vH as a key modulator of social reward contextual representations and memory.

Animals must be able to detect and discriminate stimuli according to their valence to support adaptive behaviour and memory processes. In various species, chemosensory cues from females are considered naturally rewarding and highly attractive to males, resulting in the activation of the dopaminergic reward system[46]. In our study, sexually naïve males were exposed to female odorant/pheromonal stimuli through the soiled bedding of unfamiliar females in a context-dependent manner. While the ventral CA1 and dorsal CA2 regions of the hippocampus are known to store social memories of conspecifics[13,20,21,47,48], much less is understood about whether the vH forms selective representations of social reward contexts and the underlying neuronal dynamics and circuits.

We discovered that a population of vH neurons, i.e., the social reward context neurons, selectively activate in the social reward context following learning, consistent with the fact that the hippocampus (both its dorsal and ventral subdivisions) displays context-specific activity patterns after reward conditioning[18,40,49,50]. Social reward contextual learning led to a reorganization of the context-selective activity of vH neurons, consistent with the former studies showing that vH neurons remap their spatial firing activity in the presence of unconditioned olfactory cues, such as predator odour[18], as well as odours associated with reward[19]. Specifically, in a biconditional odour discrimination task involving sucrose rewards in two distinct contexts, vH CA3 neurons were found to be originally active across both contexts but became context-selective as animals learned the odour-reward contingencies[19]. Similarly, we found that a large proportion of vH neurons that did not discriminate contexts prior to conditioning, displayed selective activation in the social reward context at the memory test. Furthermore, disrupting vH neuronal activity during learning prevented the development of this social reward context selectivity.

Early observations that information is more readily recalled in the environment where learning had occurred led to classical psychological theories on the ability of spatial contexts to regulate memory

https://doi.org/10.1038/s41467-024-53866-2

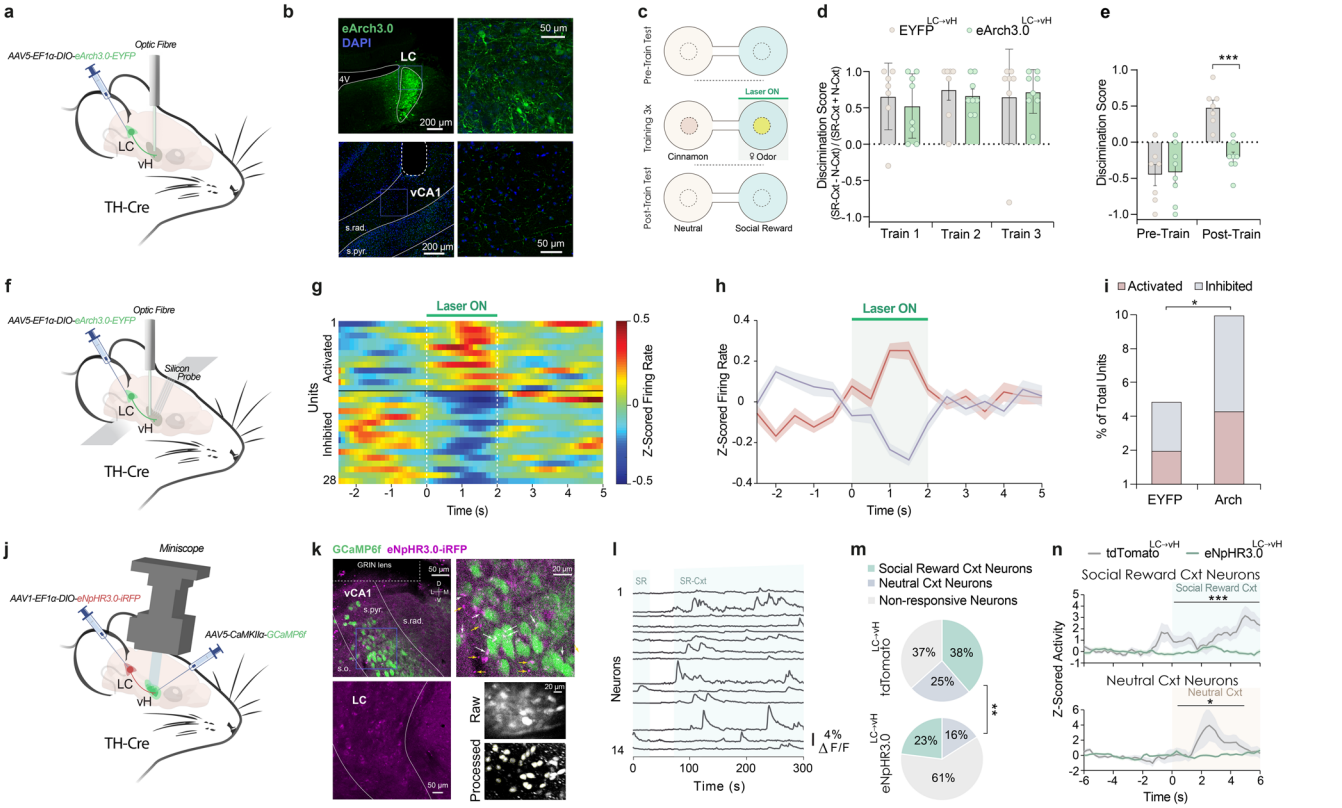

Fig. 6 | Social reward contextual memory involves locus coeruleus projections to the vH. a Schematic of optogenetic inhibition of LC→vH terminals. (A-E) EYFP: $n = 7$; eArch3.0: $n = 8$ mice. **b** Images of eArch3.0 expression in LC soma and projections in vH. Expression was verified for all 15 mice. **c** Optogenetic inhibition protocol during SR CPP training. **d** Behavioural discrimination score at training. Two-way Mixed-ANOVA, no group effect $F_{(1,7)} = 0.17$ $P = 0.69$. **e** Discrimination score at Pre- and Post-train. Two-way Mixed-ANOVA, group × session $F_{(1,5)} = 11.33$ $P = 0.020$; Bonferroni-corrected 2-tailed t-test, Post-train EYFP vs. eArch3.0 $P = 0.0313$. **f** Schematic of eArch3.0 expression in LC neurons, and optic fibre and silicon probe in vH. **g** Trial-averaged responses of laser-activated and -inhibited neurons in vH of eArch3.0$^{LC→vH}$. Dashed lines mark laser onset/offset. **h** Averaged responses across trial time. **i** Percentage of neurons activated or inhibited by LC→vH terminal inhibition. Chi-squared test, $\chi^2_{(1,\ N\ =\ 593)} = 5.73$ $P = 0.0166$. (F-I), EYFP$^{LC→vH}$ $n = 311$ neurons from 4 mice, eArch3.0$^{LC→vH}$ $n = 282$ neurons from 3 mice. **j** Simultaneous optogenetic inhibition of LC projections and in vivo calcium imaging from vH pyramidal neurons. **j**–**n** tdTomato: $n = 84$ neurons, 2 mice; eNpHR3.0: $n = 179$ neurons, 2 mice. **k** Images of eNpHR3.0 expression in LC soma (bottom left), LC→vH projections and GCaMP6f in vH pyramidal neurons (top left, right). Yellow arrows: LC varicosities, white arrows: LC varicosities superimposed on GCaMP6f+ pyramidal neurons. Bottom right, raw and processed images of 1-photon calcium signals in vH pyramidal neurons. Expression was verified for all 4 mice. **l** Calcium traces of pyramidal neurons during Post-Train. **m** Proportions of SR-context neurons during Post-Train. Chi-squared test, $P = 0.0096$. **n** Z-scored calcium activity upon entry into the SR- or neutral-context during Post-Train. Top, two-way Mixed-ANOVA, pre-entry group × time $F_{(2.3,163.9)} = 3.98$ $P = 0.016$; post-entry group $F_{(1,71)} = 13.65$ $P = 0.00043$. Bottom, two-way Mixed-ANOVA, post-entry group × time $F_{(1.65,77.46)} = 3.82$ $P = 0.034$. Data are presented as the mean ± SEM.

retrieval[51]. Strikingly, in our experiments, the fraction of social reward context neurons correlated with contextual memory retrieval, suggesting that hippocampal contextual representations imbued with positive value influence the strength of memory retrieval. Of note, we observed that roughly 30% of vH neurons were activated by soiled bedding containing female odours and pheromones, and that a large proportion of these neurons also respond to sucrose and a female conspecific. This suggests that female odour is represented as both rewarding and social in the vH of male mice. The social reward responsiveness of vH neurons indicates that converging information from odour-driven long-range synaptic inputs to the vH, such as from the piriform cortex[52], as well as other inputs from brain regions coding social salience, such as the amygdala[53], and dCA2[20], could instruct vH contextual representations during learning. Although a significant fraction of vH neurons were activated by female odour, silencing vH activity in the vicinity of this stimulus did not alter exploration behaviour while impairing subsequent place preference, suggesting that the vH is predominantly involved in encoding spatial information associated with a social reward.

Contextual representations in the hippocampus are thought to be transmitted to downstream regions where they are integrated with stimulus identity, associated values, and behavioural outcomes[54]. Our lab and others have found spatial and valence coding in the ventral hippocampus[40,43,55–58], hinting at the possible confluence of the animal's current location in space and its emotional state. Notably, vH neurons exhibiting context-dependent representations following learning did not significantly overlap in paradigms of opposite valence, in line with previous studies showing functional heterogeneity within vH pyramidal neurons and their projection targets[24,59,60]. The social reward and fear learning tasks also differed by the social and non-social nature of the stimuli, potentially contributing to the distinct neuronal representations observed. However, to our knowledge, a vH projection circuit specifically encoding social information, independent of valence, has yet to be identified. We predict that these contextual- and valence-specific neuronal representations in the vH likely diverge in their long-range synaptic targets. Consistent with this prediction and to support context-mediated emotional memory selection, social reward context neurons in the vH may preferentially project to the NAc[12,13,15,40], or medial prefrontal cortex[21,48], to signal that the context is rewarding in nature, while fear context neurons may preferentially target the basolateral amygdala[14,22], to signal that the context is aversive. Thus, selective contextual representations of positive and

negative emotions in the vH may gate or even facilitate adaptive behavioural responses mediated by downstream structures.

It is widely established that the LC is the primary source of noradrenaline in the brain, with several studies showing the impact of the LC noradrenaline system on cognitive and behavioural processes, such as the regulation of attention and working memory, goal-directed and motivated behaviour, and emotional memories[27,61]. There is also evidence that dopamine released by LC neurons in the dorsal hippocampus is critical for memory formation[29,37–39]. Additionally, former studies showed that dopamine plays a role in the manifestation of male sexual behaviour in terms of motivation and copulatory ability[3,4]. In our study, suppressing LC activity in the vH impaired the formation of social reward contextual representations and memory without affecting motivation to approach the social reward zone or context during learning. Instead, LC-vH inhibition may have disrupted the association of the social reward stimulus with the animal's contextual location.

The release of noradrenaline or dopamine from the LC can have several implications for the function of vH circuits and the formation of emotional memories. One possibility is that these neuromodulators fulfil a pure gain-control function to signal stimulus intensity thereby regulating learning strength. Successful learning requires plasticity mechanisms at the level of single neurons and synapses, which are thought to lead to the stabilization of place fields to mediate spatial memory formation[62–66]. The hippocampus contains dopamine and adrenergic receptors whose activation by their corresponding neurotransmitters promotes changes in synaptic efficacy, thus contributing to memory formation and consolidation[33,36,65,67–73]. The role of noradrenaline in learning is further supported by results showing that the stimulation of LC projections to the dorsal hippocampus promotes spatial learning[28,29], and in the case of spatial reward learning, prompts place cell enrichment adjacent to the reward location[39]. Altogether, and in line with the literature, our study suggests that LC transmission to the vH promotes the emergence of spatial representations in the social reward contextual conditioning paradigm. Yet, future studies are needed to evaluate which neuromodulators released by the LC are involved in the contextualization of a social reward memory. A potential study could employ genetically-encoded dopamine and noradrenaline receptor-based sensors combined with in vivo fibre photometry recordings to measure extracellular levels of dopamine and noradrenaline in the vH as mice undergo the social reward conditioned place preference task.

Finally, we found that LC projections to the vH were necessary for associating contexts with a social reward but not with a non-social aversive stimulus. These results were rather unexpected as there is evidence of the involvement of the LC in fear memory[37,74,75]. For instance, during auditory fear conditioning, optogenetic inhibition of the LC coinciding with shock delivery impaired fear learning[75], while pharmacogenetic activation of noradrenergic neurons in the LC has been found to induce fear relapse[74]. In our study, LC projections to the vCA1 were targeted rather than neurons in the LC. The absence of behavioural effects in contextual fear encoding are consistent with a previous study that inhibited LC input to the dorsal CA1[38]. However, a caveat to consider in our experiments is that the social reward CPP and contextual fear conditioning procedures differ in nature. In the social reward CPP paradigm, mice were exposed to both contexts simultaneously and could freely choose which context to explore. In contrast, in the contextual fear conditioning paradigm, the contextual exposures to Context A and B were separated in time and space. This may suggest that LC projections to the vH may be crucial for behaviours involving an approach-avoidance conflict as in the social reward CPP paradigm. Another caveat is that the foot shock stimulus may be more strongly perceived than the social reward stimulus, leading to the formation of more fear-context neurons in the vH, which would be sufficient for intact learning. Consistent with this idea, our contextual fear conditioning paradigm led to the formation of more fear context neurons (roughly 60%) compared to social reward context neurons (roughly 40%) in the social reward CPP paradigm. To elucidate the role of LC projections to the vH in social reward contextual memory, future studies should employ contextual place avoidance tasks with both non-social and social aversive stimuli.

In conclusion, our observations together with prior studies identify the vH as a crucial node for contextual emotional memories as part of a wide-ranging neuronal circuitry integrating converging spatial and emotional information. Our study, in mice, provides insight into how spatial contextual representations in the hippocampus are imbued with emotional values to ensure context-dependent memory selection. These findings may have implications for neuropsychiatric disorders like substance abuse or post-traumatic stress disorder, where the improper linking of emotional stimuli to the environment leads to maladaptive behaviours that are excessive or indiscriminate[76].

Methods

Mice

Male C57BL/6 J mice (Janvier Labs, France) or tyrosine hydroxylase Cre mice (Jackson Laboratories, B6.Cg-7630403G23RikTg(TH-Cre)1Tmd/J) aged 3–4 months old were used for experiments. Mice were grouped housed (2–4 mice per cage) in a 12 h light/dark cycle and provided with food and water ad libitum. Mice used for electrophysiology experiments were individually housed beginning 3 days before surgery. All behavioural experiments were conducted during the light cycle. All animal procedures were executed following institutional guidelines and were approved by the prescribed authorities (Veterinary Office of the Canton of Bern, Switzerland).

Surgery

Mice were anaesthetized with isoflurane (induction 3%, maintenance 1.5%) in oxygen at a flow rate of 1 L/min throughout the procedure. Core body temperature was kept at 37 °C by a feed-back controlled heating pad (Harvard Apparatus GmbH, Breisgau, Germany). Ophthalmic cream was applied to avoid eye drying. The mice were positioned into a stereotaxic frame (David Kopf Instruments, California, USA), and local analgesia was applied by injecting a mixture of 2% of lidocaine (Streuli Pharma, Uznach, Switzerland) and 0.5% bupivacaine (Aspen Pharma Schweiz, Baar, Switzerland) subcutaneously under the scalp. Anaesthesia was confirmed by detecting deep breathing, slow heart rate, and lack of the toe pinch reflex. The skull was uncovered after a skin incision, and Bregma and Lambda were aligned. A craniotomy was made on the skull above the region of interest. The dura matter was removed, and saline solution and haemostatic porcine gelatin sponges (Equimedical) were applied to the brain surface to avoid edemas.

In vivo electrophysiology. C57BL6/J mice were unilaterally implanted in the vH with a custom-made microdrive (Axona Ltd, St Albans, UK) holding eight tetrodes targeted at the following coordinates: AP 3.0 mm, ML ± 3.1 mm, DV 4–4.3 mm from the bregma. The tetrodes consisted of eight individually insulated, gold-plated tungsten wires (12.7 μm inner diameter, impedance 100–300 kΩ, California Fine Wire Company, California, USA) and were placed in a stainless steel guide cannulas and attached to a 32-pin connector (Omnetics Connector Corporation, Minnesota, United States). Two stainless steel screws implanted above the cerebellum were used as ground electrodes. Next, the exposed parts of the tetrodes were protected using sterile wax. Then the microdrive was fixed to the skull with light-cured dental adhesive (Kerr, OptiBond Universal, Kloten, Switzerland) and dental cement (Ivoclar, Tetric EvoFlow, Schaan, Principality of Liechtenstein). Mice were given Carprofen (5 mg/kg, subcutaneous) for three days after surgery.

Optogenetics experiments. The LC (AP −5.45 mm, ML ± 0.9 mm, DV −3.65 mm from Bregma) of TH-Cre mice were injected bilaterally into the with AAV2/5-EF1α-DIO-eArch3.0-EYFP or AAV2/5-EF1α-DIO-EYFP (both viruses from UNC vector core, 0.3 µl of viral solution, viral titre: $1x10^{13}$ GC/ml) via a glass micropipette (Blaubrand, Brand, Wertheim, Germany) and a microinjector Picospritzer III (Parker Hannifin, Ohio, USA). The micropipette was left in place for 10 min after infusion to avoid backflow. Optic fibres were lowered into vH at coordinates of AP 2.9 mm, ML 3.3 mm and DV −4.0 mm at at low speed of 1 mm/min. Optic fibres were constructed by gluing a piece of multimodal optical fibre (200 µm, 0.37 NA, Thorlabs, New Jersey, USA) to a 1.25 mm diameter, 230 µm bore ceramic ferrule (Senko, Pennsylvania, USA). The optic fibre implants were secured to the skull with stainless steel screws and light-cured dental adhesive and dental cement. Mice were allowed to recover for at least four weeks before behavioural assays to ensure sufficient expression of the viral construct.

Calcium imaging. Mice were unilaterally injected in the LC (AP −5.45 mm, ML ± 0.9 mm, DV −3.65 mm from Bregma) with AAV1-EF1α-DIO-eNpHR3.0-iRFP (University of Zurich viral vector facility, viral titre: 6.7×10^{12} vg/ml) or AAV8-EF1α-Flex-tdTomato (UNC vector core, viral titre: 1×10^{13} GC/ml) using a glass micropipette (0.3 µl of viral solution). The micropipette was left in place for 10 min after infusion and then slowly retracted to avoid backflow. Then, mice were injected with 0.5 µl of AAV2/5-CaMKIIα-GCaMP6f (Addgene, #100834), viral titre: 1×10^{13} vg/mL) into the vH (AP −3.28 mm, ML + 3.45 mm, DV −4.0 mm from Bregma). The micropipette was left in place for 45 min after infusion. Three skull screws were inserted around the implantation site. The GRIN lens (0.6 mm diameter) was slowly lowered to DV −4.0 mm by using a leading 21 gauge needle attached to a custom-made stereotaxic guide that allowed precise placement of the lens. The lens was fixed to the skull surface with light-cured dental adhesive and dental cement. The dorsal surface of the skull and the three bone screws were cemented with the GRIN lens to ensure the implant's stability.

Three weeks later, mice with suitable virus expression were fixed in a stereotaxic frame under anaesthesia to attach an aluminium baseplate for the miniscope above the GRIN lens. After finding the best field of view, the baseplate was cemented to the skull and a cap was used to protect the GRIN lens from dust. Mice wore a dummy miniscope for 1 week to adapt to the additional weight on the head before behavioural tests and calcium signal recordings.

Behaviour

Behavioural tests were conducted under room lighting (100 lux) and recorded with an overhead webcam video camera at 30 Hz. Tracking and scoring were done using ANY-maze (Stoelting, IL, USA). Between behavioural sessions, mice stayed in their home-cages in a sound-attenuating chamber.

Social place preference conditioning. This paradigm was implemented in a two-chamber apparatus made of dark grey plastic and consisting of two circular contexts, each measuring 25 cm in diameter, joined together with a 10 cm narrow middle chamber. Each context had either black and white vertical stripes or all-white wall patterns and different textured floors. The social conditioning place preference test protocol was adapted from[3] and consisted of three stages conducted over two days: on day 1, (1) a 10-min habituation session in which an 8.5 cm diameter petri dish containing clean woodchip bedding was placed in the centre of each context to evaluate side preferences; (2) two hours later, three 10 min learning sessions separated by 1 h, in which female-bedding was presented in the non-preferred context (social context) and clean bedding mixed with a neutral odour (1% of cinnamon[77]), in the other context (non-social context); and on day 2, (3) a 10-min memory test session in which clean bedding was placed in both contexts. The apparatus was cleaned with 70% ethanol solution and dried between sessions. The time spent in each context was used to calculate a discrimination score as follows: time in social context minus time in non-social context divided by their sum. Positive values showed that the animal exhibits a preference to the social context. Twenty-three mice were used in the social place preference conditioning paradigm (compared to 24 mice in contextual fear conditioning) because one animal exhibited poor exploration due to cable twisting and was thus removed from the analysis.

A subset of mice was exposed to a mock 'conditioning' procedure prior to the social place preference conditioning protocol. This mock 'conditioning' paradigm used a two-chamber apparatus of the same size as previously described, however, with squared shapes with different visual patterns on walls and textured floors. Experiments were performed in a different position in the room exposing mice to different landmarks. The neutral 'conditioning' protocol used clean bedding mixed with 1% of rosemary in one context and clean bedding mixed with 1% of saffron in the other context during the three learning sessions. The rest of the protocol was identical to the social place preference conditioning.

Contextual fear conditioning. This behavioural paradigm took place in two different squared contexts of transparent Plexiglas (26 × 26 cm). These two contexts displayed different floor textures (grid vs. smooth floor), wall patterns, distal cues, and odours (70% ethanol or 1% acetic acid). The fear context contained a grid floor made of stainless steel rods through which scrambled electrical shocks were delivered by a shock controller (Coulbourn Instruments). Foot-shock intensity was adjusted to 0.5 mA before each experiment. The two arenas were cleaned before and after each session with 70% ethanol or 1% acetic acid, respectively.

Mice were first habituated to the two contexts (A and B) in 10-min sessions separated by a 1 h interval. Two hours later, mice were placed in the fear conditioning context (A) and received five electrical foot-shocks (0.5 mA, 1 s duration, pseudo-randomized between 30–120 s, mean 60 s) delivered through the floor grid. Four hours later, mice were tested for contextual fear memory by returning them to the fear conditioning context (A) for 10 min. Two hours later, mice were placed into the neutral context (B) to assess the animal's ability to discriminate the contexts. Freezing levels were automatically detected by ANY-maze software which tracked body positions at 30 Hz.

A subset of mice was exposed to a mock 'conditioning' procedure followed by the classical contextual fear conditioning paradigm. In the mock 'conditioning' paradigm, the contexts had equivalent dimensions with one context being circular in shape and differed in their visual cues and floor texture. In this mock conditioning paradigm, mice received two weak foot-shocks of 0.06 mA. The rest of the protocol was identical to the contextual fear conditioning protocol. Following mock 'conditioning', the mice were subjected to the classical contextual fear conditioning paradigm as previously described.

US experiments. The protocol starts with on day 1, (1) a 10-min habituation session in which an 8.5 cm diameter petri dish containing clean woodchip bedding was placed in the centre of each context to evaluate side preferences; (2) two hours later, sucrose-pellets were presented in the non-preferred context (reward context) and regular chow in the other context (neutral context). After 1 h break, female bedding was added in the reward context and clean bedding mixed with a neutral odour (1% of cinnamon[77]) in the neutral context, 1 h later a female conspecific was added in the reward context and a novel object was added in the neutral context. Upon a 1 h break predator odour (1% of TMT mixed in clean bedding) was added in the reward context and wood ships in the neutral context. After 1 h break, the animals were exposed to context A from the contextual fear conditioning task where the animals were exposed to five electrical foot-shocks (0.5 mA, 1 s duration, pseudo-randomized between 30–120 s, mean 60 s) delivered

through the floor grid. The apparatus was cleaned with 70% ethanol solution and dried between sessions.

Single-unit electrophysiological recordings in freely-moving mice

Single-unit electrophysiological recordings were performed on chronically implanted mice. After recovery from the microdrive implantation surgery, each animal was familiarized with the testing room and handling procedures which involved cable tethering to the recording system. Tetrodes were progressively lowered to the vH pyramidal layer over several days by using sharp-wave ripples and theta oscillations as electrophysiological hallmarks. Twenty-four hours later, mice underwent behavioural testing as defined above. Electrophysiology and behavioural tracking data were synchronized using TTL signals sent by Anymaze to the recording system to timestamp single-camera frames or shock delivery –in the case of the contextual fear conditioning procedure.

The electrophysiological data were acquired using an Intan RHD2000 Evaluation Board and 32 channel headstage at a sampling rate of 20 kHz. The signal was amplified and a band-pass filter (500–5000 Hz) was applied offline to extract the spikes. Spikes were identified using a threshold of 5 standard deviations above the root mean square signal (0.2 ms sliding window) of the filtered signal. 32 data points (1.6 ms) were sampled for each spike waveform.

Principal component analysis (PCA) was applied to the waveforms to extract the first three components per tetrode channel. Identified spikes were automatically sorted using KlustaKwik (http://klustakwik.sourceforge.net/) followed by manual adjustment of the clusters using the software Klusters (http://neurosuite.sourceforge.net/) to acquire well-isolated single-units based on temporal cross-correlations, spike waveforms and refractory periods. The stability of single-units was confirmed by inspecting spike features throughout the recording sessions.

Head-fixed silicon probe recordings

Animals were trained 1–2 weeks before the recordings in a wheel in a dark room. Recordings were aimed at the right ventral CA1 hippocampus and recording sessions lasted between 20–30 min. Extracellular single-unit electrophysiological signals were recorded with silicon probes (Takahashi probe, 2 shank acute). For optogenetic LC terminal inhibition in vH, light pulses were delivered 33 times with 2 s on and 8 s off. Significantly responsive neurons were categorized by a Mann–Whitney *U*-test on firing rate during laser delivery (0–2 s) and pre-delivery (−3 to −0.5 s) across 33 trials.

Calcium imaging

Imaging sessions in freely-moving mice began five days after baseplating. Mice were briefly anaesthetized (<2 min) to attach the miniscope to the baseplate for each imaging day. Mice were allowed to recover from the brief anaesthesia for 60 min before the behavioural protocol started. Calcium imaging was performed using a custom-made dual-colour miniscope capable of simultaneous calcium imaging and optogenetic manipulation[78]. The power of the blue laser used for GCaMP6f excitation (488 nm, Cobolt, Solna, Sweden) was set to 1 mW at the level of the miniscope objective. The power of the red-orange laser used for eNpHR3.0 excitation (594 nm, Cobolt) was set to 8–10 mW at the level of the miniscope objective. The 488 nm laser was triggered by a TTL signal from ANY-maze at the beginning of each recording session. The 594 nm laser was switched on only when the mouse entered the social reward context. Calcium imaging videos were recorded at 20 Hz as uncompressed.avi files (1000 frames per file) by using a data acquisition (DAQ) box which is triggered by an external TTL pulse from ANY-maze to allow for simultaneous acquisition of calcium imaging and behavioural videos. The excitation power for GCaMP6f was determined in prior tests based on the most optimal signal to noise ratio and was maintained throughout all the imaging/behavioural sessions. For the inhibition of vH neurons, 400 nL AAV5-CaMKIIα-eNpHR3.0-mCherry virus (UNC Vector Core, titre 5.8 × 1012 vg/mL) was used in C57BL/6 J mice and 400 nL AAV2-CaMKIIα-mCherry virus (UNC Vector Core, titre 4.7 × 1012 vg/mL) was used as control.

Optogenetic stimulation

To optogenetically manipulate LC projections to the vH (starting four weeks after viral injections), a laser (Cobolt, Solna, Sweden) generating green light (561 nm) was attached to an optical rotary joint (Doric Lenses, Québec, Canada) to support the unrestricted movement of mice during the behavioural tests. The optical rotary joint was connected to a light splitter (Doric lenses, Québec, Canada) to allow bilateral light delivery to two patch cables (Doric Lenses, Québec, Canada) which were in turn connected to the implanted optic fibres through a ferrule-sleeve system (Senko, Pennsylvania, USA). Laser light was applied continuously at a power intensity of 10–15 mW measured from the optic fibre tip. Laser illumination was automatically triggered according to the animal's location within the behavioural apparatus in a closed-loop system. Body position was tracked in real-time using ANY-maze software, which then generated TTL pulses to trigger laser delivery whenever the animal entered the social reward context. Laser power was measured with a power-metre (Thorlabs, New Jersey, USA) before each behavioural session. Before the beginning of the behavioural paradigm, mice were first connected to the patch cables for 10 min for habituation.

Histology

For electrophysiological experiments, mice were anaesthetized with isoflurane and tetrode positions were marked by electrolytic lesions (30 μA for 10 s). Then, mice were anaesthetized using an intraperitoneal injection of a ketamine/xylazine mixture (5% ketamine, Vetoquinol, Magny-Vernois, France; 2.5% xylazine, Streuli Pharma, Uznach, Switzerland). Mice were then transcardially perfused with ice-cold phosphate-buffered saline (PBS, Roche, Basel, Switzerland) followed by 4% paraformaldehyde (PFA, Carl Roth, Karlsruhe, Germany). Implanted tetrodes or optic fibres were kept in the brain for at least 24 h of post-perfusion fixation in 4% PFA at 4 °C before being detached from the brain. Subsequently, brains were removed from the skull and post-fixed for 24 h at 4 °C. Brains were sliced (50 μm thick coronal sections) using a vibratome (VT1000 S, Leica Microsystems, Wetzlar, Germany). Sections from electrophysiological or calcium imaging experiments containing the vH were examined with a fluorescent microscope (M205 FCA, Leica Microsystems, Wetzlar, Germany) using a 2.0x magnification objective. The location of the tetrodes or the GRIN lens was manually verified by comparing the location to the mouse brain atlas. If the tip of the tetrodes or the GRIN lens was not located in the vH, the animal was excluded from further analysis. Afterwards, sections were stored in PBS containing 0.05% sodium azide.

Immunohistochemistry. Free-floating sections were washed in PBS and blocked with 5% normal donkey serum (ab7475, Abcam, Cambridge, United Kingdom) in PBS containing 0.1% Triton X-100 (PBS-T) at room temperature for 2 h. Afterwards, sections were incubated with rabbit anti-GFP polyclonal antibody (1:1000, ab6556, Abcam, Cambridge, United Kingdom) or rabbit anti-RFP polyclonal antibody (1:1000, 600-401-379, ThermoFisher, Massachusetts, USA) and chicken polyclonal anti-GFP (1:1000, ab13970, Abcam, Cambridge, United Kingdom,) in PBS-T for 48 h at 4 °C followed by three washings in PBS. Then, the slices were incubated with Alexa Fluor 488 conjugated donkey anti-rabbit secondary antibody (1:1000, A32790, Invitrogen, Massachusetts, USA) or donkey anti-chicken AlexaFluor-488 (1:1000, 703545145, Jackson ImmunoResearch Laboratories, Cambridge, UK) and donkey anti-rabbit AlexaFluor-564 (1:1000, A21207, Invitrogen, Massachusetts, USA) for 2 h at room temperature. Finally, the slices were washed three times in PBS and incubated in DAPI solution (MBD0015, Sigma-Aldrich, Missouri,

USA) to label cell nuclei, subsequently washed another three times with PBS, mounted onto microscope slides with aqueous mounting medium (Aqua-Poly/Mount, Polysciences, Pennsylvania, USA) and stored at 4 °C. Immunolabelled sections were imaged with a 20x objective on a slide scanning microscope (3DHistech, Pannoramic 250 Flash II, Budapest, Hungary) or using a confocal microscope (LSM 880, Zeiss, Jena, Germany). The location of viral transduction and optic fibre implantations were then verified.

Calcium signal processing

Calcium imaging videos were analysed using a custom Matlab code[79]. Videos from multiple sessions were concatenated and down-sampled by a binning factor of 4 resulting in a frame rate of 5 Hz, and lateral brain movement was motion-corrected using the Turboreg algorithm[80]. Fluorescent traces were extracted by applying automatically detected individual cell filters based on combined principal and individual component analysis (PCA/ICA) as described previously[81]. To control for non-inclusion of split neurons in our analyses, we identified pairs of neurons with highly correlated activity (Pearson correlation > 0.7) and are spatially close (centroid distance <20 pixels) and excluded one of the neurons for each pair. Identified putative neurons were then sorted via visual inspection to select neurons with appropriate somatic morphology and Ca^{2+} dynamics consistent with signals from individual neurons.

Data analysis

Categorization of social reward context and fear context neurons. We used a bootstrap analysis to define whether individual vH neurons were significantly active in the conditioned emotional context at memory test to categorize social reward context neurons or fear context neurons. First, for each well-isolated neuron, a spike firing-by-time vector was constructed by binning its spikes in 20 ms bins and then smoothed by convolution with a Gaussian kernel (σ = 20 ms). Then, a Student's t-statistic value was calculated based on the difference in firing rate activity between the neutral context and social reward context (or fear context and its corresponding neutral context in the case of fear conditioning). This calculation was then repeated 100000 tim`es by resampling the data with replacement which led to a bootstrap distribution of resampled data. The original Student's t-statistic value was compared to the bootstrapped distribution. Neurons whose observed statistical value fell at the extremes of the surrogate distribution ($P < 0.001$) were considered as significantly responsive, with a positive value showing higher activity in the neutral context and a negative value showing higher activity in the social context or respectively in the fear context. For analysis of activity time-locked to context entry, mice which did not enter both contexts and did not exhibit trajectories meeting the criteria of a minimum of 6 s outside followed by 6 s within the social reward context were excluded. To detect neurons excited in the social reward zone (i.e., petri dish zone containing female bedding), we compared firing rate activity inside and outside of the social reward zone or neutral context during training using the same bootstrapped permutation method. This analysis was done only in a subset of animals ($n = 19$ mice) due to the exclusion of 4 mice that lacked behavioural videos which was necessary for defining the reward zone.

Place maps. For each neuron, place maps were generated based on the mean firing rate in each spatial bin. Only timepoints with an instantaneous velocity greater than 2 cm/s measured from the body's centre point were included for analysis. First, each spike was assigned to a 1 × 1 cm maze spatial bin. The firing rate was then calculated by dividing the number of spikes occurring in each bin with the occupancy time in that bin. The place maps were then smoothed by convolving them in the X and Y dimension with a Gaussian kernel (σ = 3 cm). Place field stability was measured by performing pixel-by-pixel Pearson's r correlations between the Pre-Train and Post-Train sessions. Only mice with a minimum of 30% of spatial bins in each context were included in the analysis.

Contextual firing rate analysis. For each neuron, the firing rate was first calculated by binning spikes in 20 ms bins and dividing by the time interval. For analysis of activity time-locked to context entries, the firing rates of individual neurons were further binned into 0.02 s intervals, then Z-scored using the mean and standard deviation of the baseline firing rate prior to context entry. For the time-locked activity in the bedding zone, a subset of animals was used ($n = 11$ mice) due to the exclusion of mice that did not enter both contexts and did not exhibit trajectories meeting the criteria of a minimum of 6 s outside followed by 6 s within the social reward context.

To calculate the normalized mean firing rate in each behavioural paradigm, a z-score was computed using the mean and standard deviation in the mean firing rates across all sessions.

Context decoding. Smoothed firing rates in 20 ms bins were obtained for each neuron in each context. For individual neurons, the firing rate was shuffled and a random sample of 60 s was selected for each context and labelled according with the context identity. The data were then randomly split (30/70) into training and hold-out test samples with a balanced number of labels. Training samples were used to train a binary linear classifier (support vector machine [SVM], Matlab Classification Learner application) with cross-validation (10-fold) and then applied to test samples with accuracy calculated as the percentage of correctly labelled samples. For the SVM calculated for individual mice, only mice with more than 10 recorded neurons were incorporated in the analysis.

Statistics

Analyses were performed using custom scripts written in MATLAB (MathWorks). Statistical analyses were carried out using Prism 9 (Graphpad software). All datasets were tested for normality using the Kolmogorov–Smirnov test. All null-hypothesis tests were two-tailed. ANOVAs were followed by post hoc tests if a main effect was observed. Post hoc multiple comparisons were done using the Bonferroni correction. Chi-squared tests were conducted to compare differences in proportions between groups. *P*-values for statistical significance are reported in the figure legends. Box and whisker plots show median, interquartile range (25th and 75th percentiles). All data are shown as mean ± S.E.M. Asterisks in the figures represent *P*-values with the following thresholds: $*P < 0.05$; $**P < 0.01$; $***P < 0.001$; $****P < 0.0001$.

Reporting summary

Further information on research design is available in the Nature Portfolio Reporting Summary linked to this article.

Data availability

Source data are provided with this paper. Datasets generated in the current study are available on Zenodo (https://doi.org/10.5281/zenodo.13770058). Source data are provided with this paper.

Code availability

Custom-written scripts used to analyse data from this study are available on Zenodo (https://doi.org/10.5281/zenodo.13770478).

References

1. LeDoux, J. E. Emotion circuits in the brain. *Annu. Rev. Neurosci.* **23**, 155–184 (2000).
2. Chen, P. & Hong, W. Neural circuit mechanisms of social behavior. *Neuron* **98**, 16–30 (2018).
3. Beny-Shefer, Y. et al. Nucleus accumbens dopamine signaling regulates sexual preference for females in male mice. *Cell Rep.* **21**, 3079–3088 (2017).

4. Dai, B. et al. Responses and functions of dopamine in nucleus accumbens core during social behaviors. *Cell Rep.* **40**, 111246 (2022).
5. Bergan, J. F., Ben-Shaul, Y. & Dulac, C. Sex-specific processing of social cues in the medial amygdala. *Elife* **3**, e02743 (2014).
6. Gunaydin, L. A. et al. Natural neural projection dynamics underlying social behavior. *Cell* **157**, 1535–1551 (2014).
7. Levy, D. R. et al. Dynamics of social representation in the mouse prefrontal cortex. *Nat. Neurosci.* **22**, 2013–2022 (2019).
8. Fanselow, M. S. & Dong, H. W. Are the dorsal and ventral hippocampus functionally distinct structures? *Neuron* **65**, 7–19 (2010).
9. Bannerman, D. M. et al. Ventral hippocampal lesions affect anxiety but not spatial learning. *Behav. Brain Res.* **139**, 197–213 (2003).
10. Britt, J. P. et al. Synaptic and behavioral profile of multiple glutamatergic inputs to the nucleus accumbens. *Neuron* **76**, 790–803 (2012).
11. Ito, R., Robbins, T. W., Pennartz, C. M. & Everitt, B. J. Functional interaction between the hippocampus and nucleus accumbens shell is necessary for the acquisition of appetitive spatial context conditioning. *J. Neurosci.* **28**, 6950–6959 (2008).
12. LeGates, T. A. et al. Reward behaviour is regulated by the strength of hippocampus-nucleus accumbens synapses. *Nature* **564**, 258–262 (2018).
13. Okuyama, T., Kitamura, T., Roy, D. S., Itohara, S. & Tonegawa, S. Ventral CA1 neurons store social memory. *Science* **353**, 1536–1541 (2016).
14. Xu, C. et al. Distinct hippocampal pathways mediate dissociable roles of context in memory retrieval. *Cell* **167**, 961–972 (2016).
15. Zhou, Y. et al. A ventral CA1 to nucleus accumbens core engram circuit mediates conditioned place preference for cocaine. *Nat. Neurosci.* **22**, 1986–1999 (2019).
16. Jung, M. W., Wiener, S. I. & McNaughton, B. L. Comparison of spatial firing characteristics of units in dorsal and ventral hippocampus of the rat. *J. Neurosci.* **14**, 7347–7356 (1994).
17. Kjelstrup, K. B. et al. Finite scale of spatial representation in the hippocampus. *Science* **321**, 140–143 (2008).
18. Keinath, A. T. et al. Precise spatial coding is preserved along the longitudinal hippocampal axis. *Hippocampus* **24**, 1533–1548 (2014).
19. Komorowski, R. W. et al. Ventral hippocampal neurons are shaped by experience to represent behaviorally relevant contexts. *J. Neurosci.* **33**, 8079–8087 (2013).
20. Meira, T. et al. A hippocampal circuit linking dorsal CA2 to ventral CA1 critical for social memory dynamics. *Nat. Commun.* **9**, 4163 (2018).
21. Phillips, M. L., Robinson, H. A. & Pozzo-Miller, L. Ventral hippocampal projections to the medial prefrontal cortex regulate social memory. *eLife* **8**, e44182 (2019).
22. Jimenez, J. C. et al. Anxiety cells in a hippocampal-hypothalamic circuit. *Neuron* **97**, 670–683 (2018).
23. Nguyen, R., Koukoutselos, K., Forro, T. & Ciocchi, S. Fear extinction relies on ventral hippocampal safety codes shaped by the amygdala. *Sci. Adv.* **9**, eadg4881 (2023).
24. Gergues, M. M. et al. Circuit and molecular architecture of a ventral hippocampal network. *Nat. Neurosci.* **23**, 1444–1452 (2020).
25. Wee, R. W. S. & MacAskill, A. F. Biased connectivity of brain-wide inputs to ventral subiculum output neurons. *Cell. Rep.* **30**, 3644–3654 (2020).
26. Palacios-Filardo, J. & Mellor, J. R. Neuromodulation of hippocampal long-term synaptic plasticity. *Curr. Opin. Neurobiol.* **54**, 37–43 (2019).
27. Sara, S. J. & Bouret, S. Orienting and reorienting: the locus coeruleus mediates cognition through arousal. *Neuron* **76**, 130–141 (2012).
28. Takeuchi, T. et al. Locus coeruleus and dopaminergic consolidation of everyday memory. *Nature* **537**, 357–362 (2016).
29. Kempadoo, K. A., Mosharov, E. V., Choi, S. J., Sulzer, D. & Kandel, E. R. Dopamine release from the locus coeruleus to the dorsal hippocampus promotes spatial learning and memory. *Proc. Natl. Acad. Sci. USA* **113**, 14835–14840 (2016).
30. Lemon, N., Aydin-Abidin, S., Funke, K. & Manahan-Vaughan, D. Locus coeruleus activation facilitates memory encoding and induces hippocampal LTD that depends on beta-adrenergic receptor activation. *Cereb. Cortex.* **19**, 2827–2837 (2009).
31. Smith, C. C. & Greene, R. W. CNS dopamine transmission mediated by noradrenergic innervation. *J. Neurosci.* **32**, 6072–6080 (2012).
32. Lin, Y. W., Min, M. Y., Chiu, T. H. & Yang, H. W. Enhancement of associative long-term potentiation by activation of beta-adrenergic receptors at CA1 synapses in rat hippocampal slices. *J. Neurosci.* **23**, 4173–4181 (2003).
33. Liu, Y., Cui, L., Schwarz, M. K., Dong, Y. & Schlüter, O. M. Adrenergic gate release for spike timing-dependent synaptic potentiation. *Neuron* **93**, 394–408 (2017).
34. Qian, H. et al. β2-Adrenergic receptor supports prolonged theta tetanus-induced LTP. *J. Neurophysiol.* **107**, 2703–2712 (2012).
35. Thomas, M. J., Moody, T. D., Makhinson, M. & O'Dell, T. J. Activity-dependent beta-adrenergic modulation of low frequency stimulation induced LTP in the hippocampal CA1 region. *Neuron* **17**, 475–482 (1996).
36. Wang, S. H., Redondo, R. L. & Morris, R. G. M. Relevance of synaptic tagging and capture to the persistence of long-term potentiation and everyday spatial memory. *Proc. Natl. Acad. Sci. USA* **107**, 19537–19542 (2010).
37. Wagatsuma, A. et al. Locus coeruleus input to hippocampal CA3 drives single-trial learning of a novel context. *Proc. Natl. Acad. Sci. USA* **115**, 310–316 (2018).
38. Chowdhury, A. et al. A locus coeruleus-dorsal CA1 dopaminergic circuit modulates memory linking. *Neuron* **20**, 3371–3388 (2022).
39. Kaufman, A. M., Geiller, T. & Losonczy, A. A role for the locus coeruleus in hippocampal CA1 place cell reorganization during spatial reward learning. *Neuron* **105**, 1018–1026 (2020).
40. Ciocchi, S., Passecker, J., Malagon-Vina, H., Mikus, N. & Klausberger, T. Brain computation: selective information routing by ventral hippocampal CA1 projection neurons. *Science* **348**, 560–563 (2015).
41. Riaz, S., Schumacher, A., Sivagurunathan, S., Van Der Meer, M. & Ito, R. Ventral, but not dorsal, hippocampus inactivation impairs reward memory expression and retrieval in contexts defined by proximal cues. *Hippocampus* **27**, 822–836 (2017).
42. Nguyen, R., Sivakumaran, S., Lambe, E. K. & Kim, J. C. Ventral hippocampal cholecystokinin interneurons gate contextual reward memory. *iScience* **27**, 108824 (2024).
43. Royer, S., Sirota, A., Patel, J. & Buzsáki, G. Distinct representations and theta dynamics in dorsal and ventral hippocampus. *J. Neurosci.* **30**, 1777–1787 (2010).
44. Cai, D. J. et al. A shared neural ensemble links distinct contextual memories encoded close in time. *Nature* **534**, 115–118 (2016).
45. Ghosh, K. K. et al. Miniaturized integration of a fluorescence microscope. *Nat. Methods* **8**, 871–878 (2011).
46. Malkesman, O. et al. The female urine sniffing test: a novel approach for assessing reward-seeking behavior in rodents. *Biol. Psychiatry* **67**, 864–871 (2010).
47. Hitti, F. L. & Siegelbaum, S. A. The hippocampal CA2 region is essential for social memory. *Nature* **508**, 88–92 (2014).
48. Sun, Q. et al. Ventral hippocampal-prefrontal interaction affects social behavior via parvalbumin positive neurons in the medial prefrontal cortex. *iScience* **23**, 100894 (2020).
49. Sjulson, L., Peyrache, A., Cumpelik, A., Cassataro, D. & Buzsáki, G. Cocaine place conditioning strengthens location-specific hippocampal coupling to the nucleus accumbens. *Neuron* **98**, 926–934 (2018).
50. Trouche, S. et al. Recoding a cocaine-place memory engram to a neutral engram in the hippocampus. *Nat. Neurosci.* **19**, 564–567 (2016).

51. Godden, D. R. & Baddeley, A. D. Context-dependent memory in two natural environments: on land and underwater. *Br. J. Psychol.* **66**, 325–331 (1975).
52. Poo, C., Agarwal, G., Bonacchi, N. & Mainen, Z. F. Spatial maps in piriform cortex during olfactory navigation. *Nature* **601**, 595–599 (2022).
53. Felix-Ortiz, A. C. & Tye, K. M. Amygdala inputs to the ventral hippocampus bidirectionally modulate social behavior. *J. Neurosci.* **34**, 586–595 (2014).
54. Maren, S., Phan, K. L. & Liberzon, I. The contextual brain: implications for fear conditioning, extinction and psychopathology. *Nat. Rev. Neurosci.* **14**, 417–428 (2013).
55. Forro, T. et al. Anxiety-related activity of ventral hippocampal interneurons. *Prog. Neurobiol.* **219**, 102368 (2022).
56. Malagon-Vina, H., Ciocchi, S. & Klausberger, T. Firing patterns of ventral hippocampal neurons predict the exploration of anxiogenic locations. *Elife* **12**, https://doi.org/10.7554/eLife.83012 (2023).
57. Li, K., Koukoutselos, K., Sakaguchi, M. & Ciocchi, S. Distinct ventral hippocampal inhibitory microcircuits regulating anxiety and fear behaviors. *Nat. Commun.* **15**, 8228 (2024).
58. Volitaki, E., Forro, T., Li, K., Nevian, T. & Ciocchi, S. Activity of ventral hippocampal parvalbumin interneurons during anxiety. *Cell Rep.* **43**, 114295 (2024).
59. Bienkowski, M. S. et al. Integration of gene expression and brain-wide connectivity reveals the multiscale organization of mouse hippocampal networks. *Nat. Neurosci.* **21**, 1628–1643 (2018).
60. Shpokayte, M. et al. Hippocampal cells segregate positive and negative engrams. *Commun. Biol.* **5**, 1009 (2022).
61. Poe, G. R. et al. Locus coeruleus: a new look at the blue spot. *Nat. Rev. Neurosci.* **21**, 644–659 (2020).
62. Bliss, T. & Lomo, T. Long-lasting potentiation of synaptic transmission in the dentate area of the anaesthetized rabbit following stimulation of the perforant path. *J. Physiol.* **232**, 331–356 (1973).
63. Buzsáki, G. Hippocampal sharp wave-ripple: a cognitive biomarker for episodic memory and planning. *Hippocampus* **25**, 1073–1188 (2015).
64. Martin, S. J., Grimwood, P. D. & Morris, R. G. Synaptic plasticity and memory: an evaluation of the hypothesis. *Annu. Rev. Neurosci.* **23**, 649–711 (2000).
65. Kentros, C. et al. Abolition of long-term stability of new hippocampal place cell maps by NMDA receptor blockade. *Science* **280**, 2121–2126 (1998).
66. McHugh, T. J., Blum, K. I., Tsien, J. Z., Tonegawa, S. & Wilson, M. A. Impaired hippocampal representation of space in CA1-specific NMDAR1 knockout mice. *Cell* **87**, 1339–1349 (1996).
67. Broussard, J. I. et al. Dopamine regulates aversive contextual learning and associated in vivo synaptic plasticity in the hippocampus. *Cell Rep.* **14**, 1930–1939 (2016).
68. Hu, H. et al. Emotion enhances learning via norepinephrine regulation of AMPA-receptor trafficking. *Cell* **131**, 160–173 (2007).
69. Kwon, O. B. et al. Neuregulin-1 regulates LTP at CA1 hippocampal synapses through activation of dopamine D4 receptors. *Proc. Natl. Acad. Sci. USA* **105**, 15587–15592 (2008).
70. Rocchetti, J. et al. Presynaptic D2 dopamine receptors control long-term depression expression and memory processes in the temporal hippocampus. *Biol. Psychiatry* **77**, 513–525 (2015).
71. Li, S., Cullen, W. K., Anwyl, R. & Rowan, M. J. Dopamine-dependent facilitation of LTP induction in hippocampal CA1 by exposure to spatial novelty. *Nat. Neurosci.* **6**, 526–531 (2003).
72. McNamara, C. G., Tejero-Cantero, Á., Trouche, S., Campo-Urriza, N. & Dupret, D. Dopaminergic neurons promote hippocampal reactivation and spatial memory persistence. *Nat. Neurosci.* **17**, 1658–1660 (2014).
73. Murchison, C. F. et al. A distinct role for norepinephrine in memory retrieval. *Cell* **117**, 131–143 (2004).
74. Giustino, T. F., Fitzgerald, P. J., Ressler, R. L. & Maren, S. Locus coeruleus toggles reciprocal prefrontal firing to reinstate fear. *Proc. Natl. Acad. Sci. USA* **116**, 8570–8575 (2019).
75. Uematsu, A. et al. Modular organization of the brainstem noradrenaline system coordinates opposing learning states. *Nat. Neurosci.* **20**, 1602–1611 (2017).
76. Liberzon, I. & Abelson, J. L. Context processing and the neurobiology of post-traumatic stress disorder. *Neuron* **92**, 14–30 (2016).
77. Aqrabawi, A. J. & Kim, J. C. Behavioral evaluation of odor memory in mice. *Bio Protoc.* **8**, e3023 (2018).
78. Srinivasan, S. et al. Miniaturized microscope with flexible light source input for neuronal imaging and manipulation in freely behaving animals. *Biochem. Biophys. Res. Commun.* **517**, 520–524 (2019).
79. Grewe, B. F. et al. Neural ensemble dynamics underlying a long-term associative memory. *Nature* **543**, 670–675 (2017).
80. Thévenaz, P., Ruttimann, U. E. & Unser, M. A pyramid approach to subpixel registration based on intensity. *IEEE Trans. Image Process* **7**, 27–41 (1998).
81. Mukamel, E. A., Nimmerjahn, A. & Schnitzer, M. J. Automated analysis of cellular signals from large-scale calcium imaging data. *Neuron* **63**, 747–760 (2009).

Acknowledgements

This work was supported by an ERC starting grant (716761, S.C.), and a Swiss National Science Foundation professorship grant (170654 S.C.). We thank Masanori Sakaguchi for sharing the design of dual-colour miniscope, Benjamin Grewe for the calcium analysis toolset, the members of the Ciocchi laboratory for discussions and assistance with the project, Michael Känzig for genotyping the mice and Christian Dellenbach for technical assistance.

Author contributions

J.M.D., R.N. and S.C. conceived the project and designed experiments. J.M.D. performed the experiments and collected data with the help of R.N. M.K., K.L., C.C., A.M., and T.F. performed the surgeries and conducted calcium imaging and electrophysiological experiments, optogenetic manipulation and behaviour experiments for the manuscript revisions. J.M.D. and R.N. analysed data. S.C., R.N. and J.M.D. contributed to the writing of the manuscript. S.C. acquired funding and S.C. and R.N. supervised the project.

Competing interests

The authors declare no competing interests.

Additional information

Supplementary information The online version contains supplementary material available at https://doi.org/10.1038/s41467-024-53866-2.

Correspondence and requests for materials should be addressed to Stéphane Ciocchi.

Peer review information *Nature Communications* thanks Thomas McHugh and the other, anonymous, reviewer(s) for their contribution to the peer review of this work. A peer review file is available.